Construction Robotics (2024) 8:11
https://doi.org/10.1007/s41693-024-00124-y

ORIGINAL PAPER

Concrete gyroid: an additive manufacturing (AM) method to 3D print gyroid geometries with a cementitious material

Lawson Spencer[1] · Moneeb Genedy[2] · James Strait[2] · Sriramya Duddukuri Nair[2] · Sasa Zivkovic[1]

Received: 15 December 2023 / Accepted: 28 May 2024 / Published online: 17 June 2024

Abstract
The gyroid is a triply periodic minimal surface (TPMS) that efficiently distributes stress under compressive loading in all Cartesian orientations. Despite the gyroid's geometric ability to evenly distribute load, it has yet to be more broadly introduced to concrete additive manufacturing (AM) due to the difficulty of printing steep, doubly curved overhangs with a cementitious material. Consequently, the employment of the gyroid TPMS in AM has been limited to small and nano-scale applications. However, for doubly curved 3D printed concrete (3DPC) structures, the feasibility of the print is determined by the relationship between geometry, tool path design, and the mechanical and rheological properties of the concrete material being extruded. Using a 6-axis robotic arm with an accelerator-injection extruder as an end-effector, this research examines the fabrication limitations to construct a 3DPC gyroid. The methods of this paper will present: (1) a parametric method to digitally model a gyroid TPMS through non-uniform rational basis spline (NURBS) surfaces followed by (2) a series of geometric density studies for robotic fabrication, which informed the design of (3) a continuous tool path. Using these findings, (4) several samples were printed to test the overhang limits of the 3DPC gyroid samples. Finally, one of the overhang samples was prepared for a series of compression tests, which demonstrated that the 3DPC gyroid structure could support over 1000 kilonewtons. Though large variability was observed in the performance of three gyroid samples tested, the research demonstrates that steep overhangs can be printed in concrete for gyroid-based structures.

Keywords 3D printed concrete (3DPC) · Gyroid structure · 3DPC gyroid · Concrete additive manufacturing

1 Introduction

3D printed concrete (3DPC) is an additive manufacturing (AM) method that offers new opportunities in the building construction industry to reduce onsite labor costs and onsite construction time, and minimize job site health and safety risks (Ko and Kuo 2019). Compared to cast concrete structures, 3DPC can be used to create complex, free-form structural elements quickly and accurately without the use of formwork at a range of scales (Xiao et al. 2021). Such elements can be structurally informed through various methods of optimization (Plessis et al. 2021) that can reduce the total amount of volume printed while maintaining equal or similar critical load capacity as unoptimized geometries. However, 3DPC is primarily used in the design of compressive-only structures because of the material's low tensile strength, as exhibited in many cementitious and sedimentary structures that do not possess additional reinforcement. Furthermore, it is difficult to integrate vertical rebar systems (for added tension) into the printing process because of the logistical challenge of the extruding end-effector colliding into any rebar higher than the current print layer. As such, 3DPC buildings and building components are often vertical or near vertical extrusions of the first layer of deposited material with very small-to-no overhang between layers.

The limits of the overhang are not only affected by the properties of the extruded material, but also by the geometry being printed and its tool path design. For example, it is easier to print a doubly curved dome as compared to a canted wall with the same overhang angle, because doubly curved shells evenly distribute all compression and tension forces through the shell's cross section, thereby eliminating almost all bending moments by sustaining the external

✉ Lawson Spencer
lawsonleespencer@gmail.com

[1] College of Architecture, Art and Planning, Cornell University, Sibley Hall, Ithaca, NY 14853, USA

[2] Civil and Environmental Engineering, Cornell University, Hollister Hall, Ithaca, NY 14853, USA

and gravity loads through membrane stresses (Joedicke 1963). Biologically, double curvature can be found in cellular solids, such as wood, sponge, honeycomb, trabecular bone, and foams, all of which can be found throughout nature, but also manufactured through primarily isotropic materials, such as polymers, metals, ceramics, and glass (Gibson 2003). Structures with these materials are often derivative of triply periodic minimal surfaces (TPMS), which can often be further derived from various polyhedrons. TPMS are non-self-intersecting surfaces that have three lattice vectors that remain invariant (unchanged) per each translation vector. Because most TPMS have a polyhedral base (Sadoc and Charvolin 1989), they can easily be parameterized as clusters (Al-Ketan and Abu Al-Rub 2021). Depending on the cellular structure as well as the mechanical properties of the material, these types of cellular solids are typologically either bending-dominant structures or stretch-dominant structures (Gibson et al. 2010). The gyroid is a bending-dominant TPMS that exhibits high stiffness relative to the unit cell (bounding box or volume fraction) when subjected to compression loading (Downing et al. 2021; Maskery et al. 2018). Whereas stretch-dominant TPMS exhibit high stiffness when subjected to tension loading. Compared to other TPMS typologies, a gyroid can more effectively distribute compression loading from each Cartesian orientation of the cubic unit cell (Maskery et al. 2018). Despite the gyroid's geometric ability to efficiently distribute compressive loads, it has yet to be broadly applied in 3DPC building applications. In part, this is due to the difficulty of effectively printing the steep sinusoidal overhangs, inherent to the doubly curved, cellular nature of the gyroid TPMS (Downing et al. 2021). Consequently, the employment of the gyroid has been limited to small and nano-scale AM applications such as tissue engineering, thermal management devices, and soft robotics (Al-Ketan and Abu Al-Rub 2021).

To cope with the overhang issue inherent to gyroid geometries, the researchers of this paper have (a) developed a method to parametrically define the gyroid TPMS through Non-Uniform Rational Basis Spline (NURBS)-based modeling which was used to (b) conduct a series of geometric density studies and (c) develop a continuous tool path. The continuous tool path was necessary, because (d) the mortar pump used for experimentation in this setup cannot be paused during the printing process to prevent unwanted hardening of material inside the end-effector. Additionally, the NURBS-based modeling method was used to (e) parametrically modify the degree of overhang for layer-by-layer printing in a series of physically prototyped overhang tests. One of the overhang prototypes was duplicated three times for (f) a series of compression tests. Given the material constraints and equipment defined in the Methods section of this paper, this research demonstrates a method to additively manufacture gyroid concrete structures with a continuous tool path.

2 State of the art

AM with concrete is often used in the design and construction of compressive-based structures, such as walls, columns, or vaults because of the material's inability to span large distances. Naturally, it is difficult for 3DPC assemblies to exhibit steep overhangs or cantilevers during the layer-by-layer printing process because of both its mechanical and rheological properties. This often limits 3DPC to vertical (or near vertical), extruded printed structures, especially in full-scale built projects. Additionally, the integration of rebar cages into these systems demonstrates an added logistical challenge during the extrusion process. However, starting in 2014, there is precedent by the authors and others to use 3DPC as formwork for cavities that are then filled with concrete rebar cages (Paul et al. 2018; Jipa and Dillenburger 2022; Lok et al. 2024). Additionally, others have begun to integrate tension cables into prefab 3DPC post-fabrication (Vantyghem et al. 2020; Akbarzadeh et al. 2024). Despite these advancements of casting concrete into 3DPC or post-tensioning in 3DPC, AM with concrete is limited by the degree of overhang and cantilever that is possible during the printing process. In a series of prefabricated bespoke columns, a 20° maximum limiting overhang was demonstrated based upon a series of fabrication tests (Anton et al. 2021). Research by others have demonstrated that concrete corbelled arches can be printed with a 25° overhang (Duarte et al. 2021). AM with concrete does not always need to extrude the material perpendicular to the ground plane or the layer below; rather, it can also be extruded at an angle based on the friction coefficient between extruded layers. In the fabrication of the 3DPC masonry arch bridge, *Striatus,* the researchers determined a maximum overhang angle of 25° between the first and last layers printed to be the limiting angle (Dell'Endice et al. 2023). Using a similar robotic print method, others have demonstrated that corbelled arches can be printed with a cementitious material with a general overhang angle of 37° and a local maximum overhang of 60° at the top of the arch (Carneau et al. 2019). The same group of researchers also demonstrated that 45° overhangs could be printed for domes with a square base as part of their investigation into printing Nubian vaults with 3DPC (Carneau et al. 2019). In additive manufacturing, Nubian vaults are created by printing a mound of material to create a slope (around 30°–45° off of the horizontal) from which subsequent extruded material can be continuously added to create a barrel vault, and thus, each layer of the vault is supported by the previous layer and the catenary arch shape the current layer (Duarte et al. 2021; Carneau et al. 2019;

Darweesh et al. 2024). A gyroid with uniform x, y, and z scaling has an overhang of 45°, making it difficult and previously unreported to be constructed in concrete AM (Liu et al. 2022). Another TPMS, the Schwartz-D, or Diamond, discovered by Alan Schoen, was recently 3D printed as a series of prefab 3DPC sections that were post-tensioned into a concrete canopy, *Diamanti,* with a maximum overhang angle of 35° (Akbarzadeh et al. 2024).

As mentioned before, the gyroid has some geometric structural advantages (Gibson 2003; Gibson et al. 2010; Downing et al. 2021; Maskery et al. 2018) making it an attractive investigation for AM with concrete. To address the overhang issue of the gyroid geometry, others have 3D printed PLA molds and then cast concrete to develop a concrete gyroid (Nguyen-Van et al. 2020). Additionally, researchers at Autodesk have used fiber-reinforced polymer (FRP), to 3D print a cantilevering bridge with a gyroid infill (Wakefield 2022). In addition, others have used parametric models to simulate geometric density tests for various TPMSs by changing the thickness of the digital mesh through gradient transformations (Al-Ketan and Abu Al-Rub 2021; Zhang et al. 2017). Changing the thickness of the gyroid mesh assumes that one can calibrate the control of material flow rate relative to the travel speed of the nozzle. In the research presented in this paper, these variables were left constant.

3 Materials and methods

The gyroid and other similar cellular solids can be found in nature as efficient, bending-dominant structures (Plessis et al. 2021; Gibson 2003). Because the gyroid TPMS effectively distributes stress under compression loading (Downing et al. 2021), this research both investigates and presents the methods whereby the gyroid geometry can be employed in AM with concrete. Section 3.1 describes a surface-based modeling method used to construct a single gyroid unit. This method was then applied to a series of geometric density studies based on the dimensions of the toolpath (Sect. 3.2). Next, in Sect. 3.3, the design of a continuous tool path was based on the materials and equipment described in Sect. 3.4, to conduct a series of overhang tests (Sect. 3.5). One of the samples from the overhang tests was reproduced in a group of three for compression testing; the findings of such are reported in the results of the paper.

3.1 NURBS-based gyroid development

Alan Schoen developed the following trigonometric equation (Eq. 1) to approximate a gyroid (Schoen 1970):

$$\sin x\cos y + \sin y\cos z + \sin z\cos x = 0. \quad (1)$$

Equation 1 can be used to generate an isosurface in which the resulting gyroid is uniform in all three Cartesian directions: x, y, and z (Downing et al. 2021; Li et al. 2022). Isosurfaces are derived from weighted points in space, such that points with smaller values are culled and points with the highest values are used to define a mesh. The accuracy of the isosurface is determined by the density and number of points within a given volume. Because the mesh developed from the isosurface is an approximation, designing through isosurface methods can limit the number of variables, one can use to parametrically modify the gyroid. Such variables might include non-uniform scaling of the geometry in one direction, twisting, or bending the geometry, or joining the gyroid geometry to other digital geometries. However, others have used the isosurface method to parameterize a change in mesh thickness for gyroid TPMSs (Viswanath et al. 2022). Due to the limitations produced through the isosurface methods, it is better to develop the gyroid through individual NURBS curves and surfaces that can be parametrically arrayed and transformed by an associated local Cartesian cube (unit cell or bounding box). Additionally, designing through surfaces guarantees a uniform mesh construction for conducting a linear finite-element analysis (FEA) (Flores-Jimenez et al. 2022). Figure 1 illustrates the

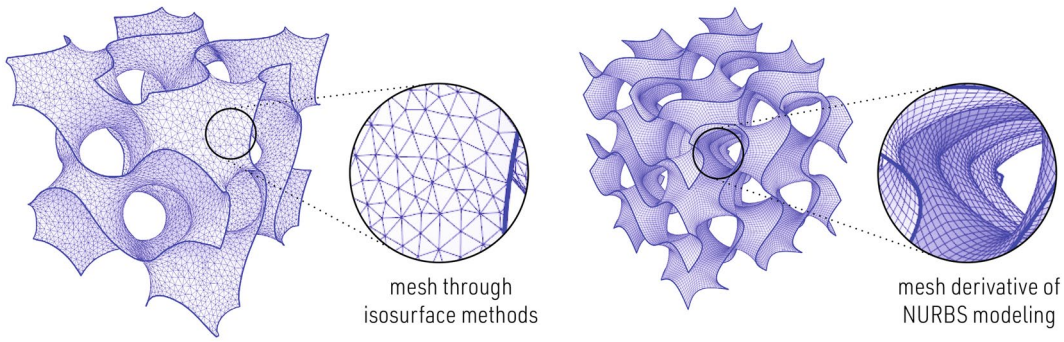

Fig. 1 Gyroid geometry through isosurface modeling methods (left) vs. NURBS modeling methods (right)

differences in gyroid TPMS meshes modeled through isosurface methods vs NURBS-based modeling methods. The advantages of modeling gyroid TPMSs through NURBS as opposed to isosurfaces have also been reported by others (Flores-Jimenez et al. 2022; Yabanigül and Yazar 2021). However, both papers describe methods that employ a "fundamental patch" to fit an approximate NURBS surface to a region of the gyroid by which the rest of the gyroid can be derived through geometric transformations. This "fundamental patch" is the smallest portion of the TPMS from which the whole gyroid can be constructed using Weierstrass parameterization (Flores-Jimenez et al. 2022; Gandy and Klinowski 2000). The fundamental patch was the base portion of a circum-helix around the central axis of the gyroid TPMS from which a warped mesh grid of 20 quadrilaterals and 5 triangles was used to compute the exact fundamental patch (Gandy and Klinowski 2000). The fundamental patch method described by Gandy and Klinowski illustrates a near exact method of representing the gyroid TPMS through 96 fundamental patches, totaling in 960 mesh faces. However, if the fundamental patch can be described through a single NURBS surface, then the resulting gyroid TPMS can be more accurately modeled through 48 surfaces, and the derivative mesh can be any number of mesh faces according to one's desired mesh resolution. The naked edges of the mesh derived from NURBS-based modeling would all be planar on one of the bounding box faces; this would not inherently be the case using an isosurface modeling method. Thus, the naked edge of the mesh derivative from an NURBS-based geometry will always be more refined than those derivative of isosurface modeling methods. Section 3.3 illustrates the use of other digital geometry that are joined to the NURBS-based gyroid TPMS to create a continuous toolpath. Joining such geometry together would not be so feasible or accurate had the gyroid been created through isosurface methods leading to patches in the geometry and thereby potential gaps in the resulting tool path.

A gyroid TPMS can be constructed through x, y, and z sine curves. A single gyroid unit has a wavelength of $2\,\pi$ in x, y, and z directions. Thus, an eighth unit of the gyroid has a length of π. Figure 2a describes how the base curves of a gyroid unit can be constructed through the following equations in terms of π:

$$[x,\ \sin x, 0] = x \text{ curve}$$

$$[0, y, \sin y] = y\text{curve}$$

$$[\sin z, \pi, z] = z\text{curve}. \tag{2}$$

The above equations were used to define points in space, which were then used to create interpolated curves (Fig. 2a) using *Grasshopper,* an algorithmic modeling and coding interface for *Rhino3d* (Rutten 2022; Robert McNeel Associates 2022). The resulting curves are then rotated around the bounding box center by 180° (Fig. 2b) and then mirrored along the xy plane at the center of the bounding box (Fig. 2c). Finally, a series of arcs are drawn perpendicular to the center of each of the curves shown in Fig. 2c following a cosine function (Fig. 2d). This is the base eighth unit of the gyroid has an x, y, and z length of π and is composed of 6 NURBS surfaces. Here, two of the fundamental patches described previously would equate to 1 NURBS surface. The eighth unit of the gyroid (Fig. 2e) can be rotated and

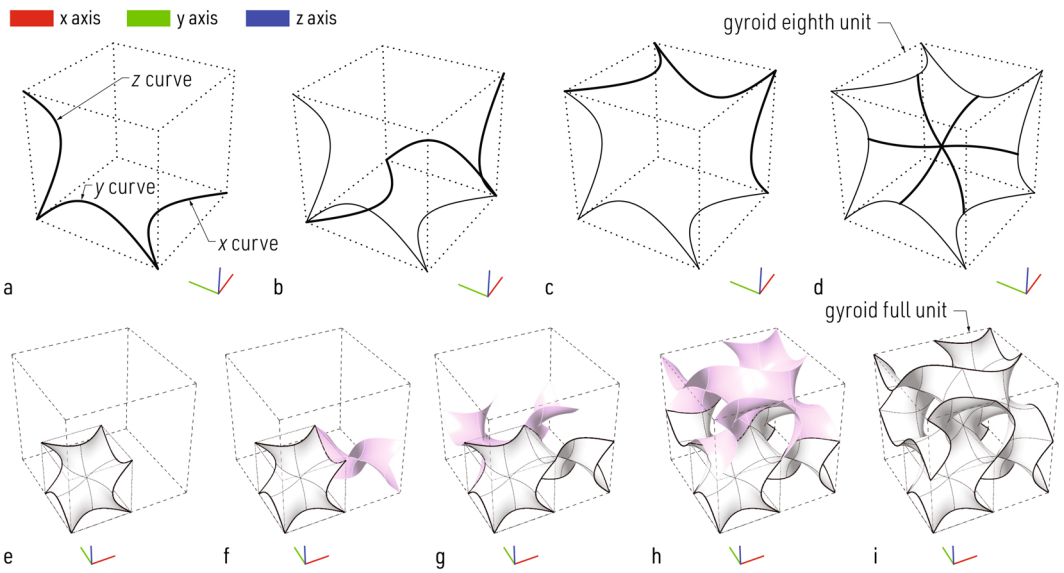

Fig. 2 Gyroid geometry creation through NURBS modeling

reoriented to complete the full unit of the gyroid (Fig. 2i). The eighth unit of the gyroid was copied in the x direction at a distance of π and rotated 180° around the xy plane at its center (Fig. 2f). The resulting two-eighth units were copied at a distance of π in the y direction and rotated 180° around the xz plane at its center (Fig. 2g). Finally, the now bottom half of the full gyroid unit was copied at a distance of π in the z direction and reflected along the yz plane at its center (Fig. 2h), thus completing the gyroid full unit (Fig. 2i). The resulting gyroid has an x, y, and z length of 2 π, and this geometry can be arrayed in all axes seamlessly joining with adjacent units. Through NURBS modeling, the single gyroid unit is composed of 48 surfaces and any meshes derived from these NURBS surfaces can have exclusively quadrilateral mesh faces.

3.2 Geometric density studies

The cross section of each layer of the extruded 3DPC was determined to be 28 mm wide by 7 mm thick based on the extruding nozzle diameter. With these layer dimensions, a series of geometric density studies were conducted within a 500 mm by 500 mm by 500 mm bounding box. Figure 3a shows one gyroid unit (2 π) within the specified bounding box. Figure 3b, c shows two and three gyroid units, respectively, within the same bounding box. The two-unit gyroid structure was selected for further investigation.

3.3 Toolpath design

For AM, concrete extruders do not often have built-in stop/start function between the pump and the end-effector, because of factors related to residual pressure overflow within hoses, changes in curing times, or the auger's relation to the accelerator injection. Due to these challenges, especially as they relate to multiple short line segments, a continuous tool path between print layers was developed for gyroid-based prints with multiples of two sine curves similar to that of previous research by the authors (Conrad et al. 2023). The continuous tool path was developed by adding additional vertical NURBS surfaces (magenta and pink in Fig. 4) to the NURBS-based gyroid (blue in Fig. 4). Figure 4 demonstrates the continuous tool path from horizontal contouring of the digital model through three critical sections within the proposed gyroid prototype. Layers 5 and 6 show a change in the tool path direction and similarly, so do layers 12 and 13. Layers 17 and 18 demonstrate a potential issue in the printing process where a 28 mm cantilever was added to the tool path in Layer 18 to make the path continuous. The added surfaces to make the toolpath continuous made up 45% of the total toolpath length for each overhang prototype. The curves along the tool path were divided into line segments no shorter than 20 mm apart. The end points of each segment were used to define the robot targets in the RAPID code.

3.4 Materials and equipment

A six-axis robotic arm, ABB Robot Model IRB 6650S (3.9 m reach, 90 kg handling capacity) on a 3.7 m linear external track, IRBT 6004 Track, and a XtreeE mortar extrusion head was used for printing the proposed gyroids, as shown in Fig. 5. A pumpable mixture with a mixture composition as shown in Table 1 and a flow diameter of 17 cm (± 1.5

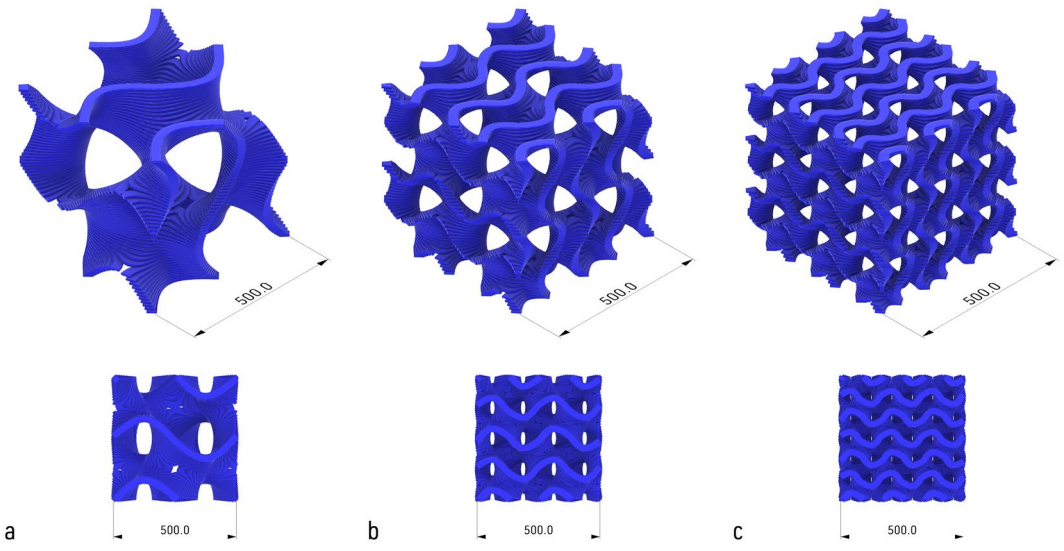

Fig. 3 Gyroid geometric density studies within a 500 mm by 500 mm by 500 mm bounding box: **a** one gyroid unit—2 π; **b** two gyroid units—4 π; **c** three gyroid units—6 π

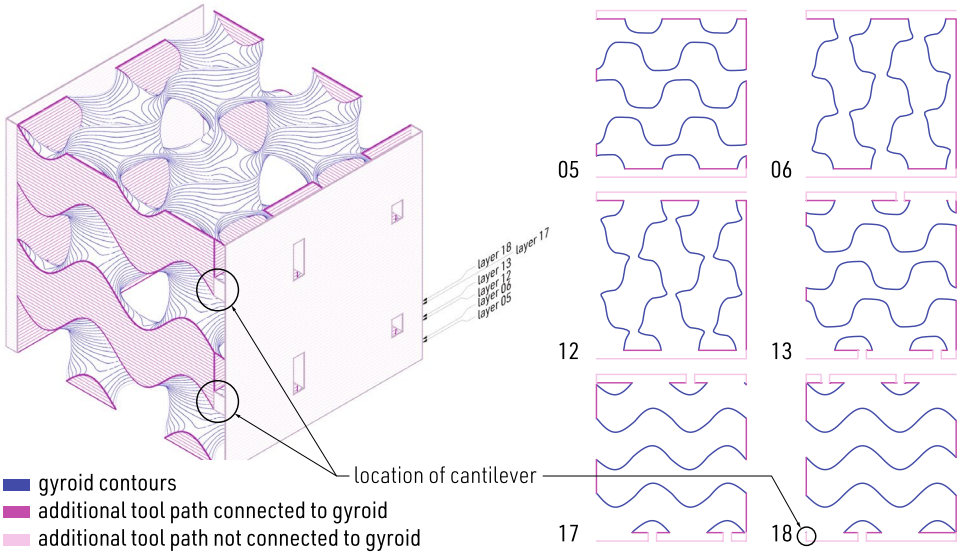

Fig. 4 Toolpath design for gyroid with 45° overhang (2 π) geometry

Fig. 5 Photo of robot printing concrete with XtreeE end-effector

Table 1 3DPC mixture design

Material*	Quantity (g)
Cement	710
Fly ash	203
Silica fume	101
Sand	1080
Water	291
HRWR	8

*Material mixture slightly adjusted during mixing process to achieve required flow

cm) was prepared in a Mortarman Mixer. The mortar mixture was then pumped through XtreeE's XFeed to achieve constant pressure at the top of the printing head of 4 bar (± 0.5 bar). The mortar was then pumped through the printing nozzle with an extrusion rate of 1.7 L/min (± 0.1 L/min). An accelerator was injected at the extrusion head at a rate of 8 mL/L of mortar and sheared prior to extruding the layer through a 20 mm nozzle. Each print had a tool path length of 325 meters and consumed 64 L of 3DPC mortar mix. A total of six batches of material were prepared for the overhang tests. Each overhang test was printed on a plywood base covered with a thick plastic sheet (Fig. 5).

3.5 Overhang tests

It is known that the early age mechanical properties of the mortar mixture along with the accelerator injection, and toolpath velocity will affect the limits of how much the deposited material can overhang. Additionally, the shape of the geometry also plays a role in the degree of overhang. Section 3.3 describes how additional surfaces can be added to the 500 mm by 500 mm by 500 mm gyroid TPMS which has a base sine curve wavelength of 4 π in x, y, and z directions (2 gyroid units in all cartesian directions). Based on this geometry, three overhang tests were designed by scaling the toolpath geometry in the z direction while maintaining a 500 mm by 500 mm bounding box. Figure 6a illustrates the no scaling in the z direction; thus, a 45° overhang angle is exhibited through the 3DPC gyroid prototype. Figure 6b, c demonstrates a 34° and 27° overhang angle relative to the vertical, respectively, by scaling the geometry in the z direction by multiples of 1.5 and 2.0. Each overhang test had 71 print layers for a total toolpath length of about 325 m and was printed at travel velocity of 153 mm/s with an average accelerator injection of 1.7 L/m. The extruding nozzle was perpendicular to the plywood base throughout the entirety

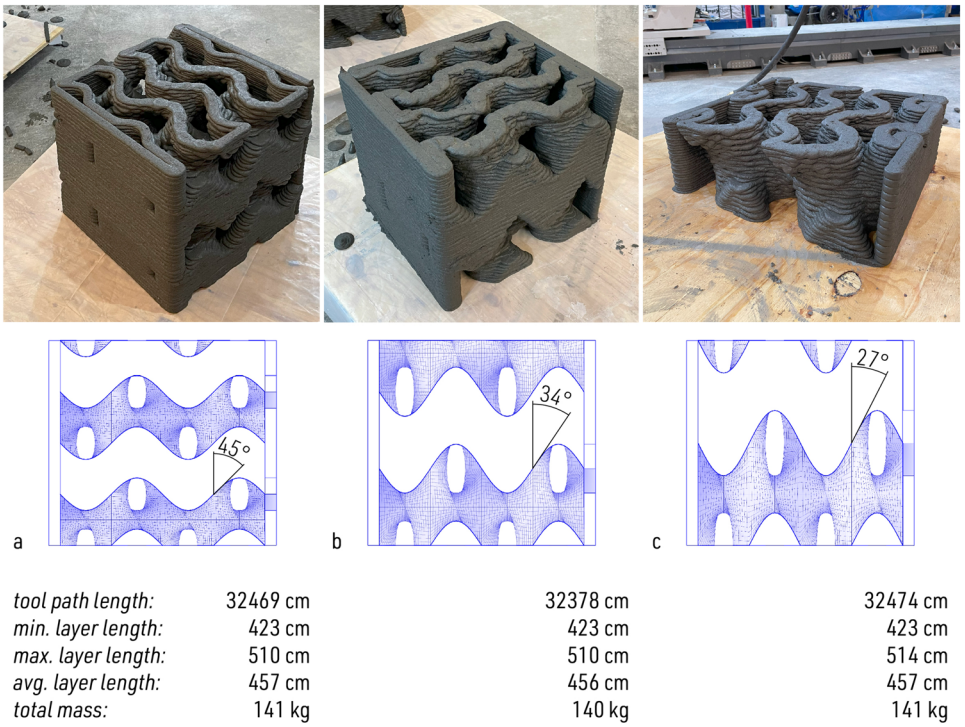

Fig. 6 Photos of overhang print tests: **a** gyroid uniformly scaled in *x, y*, and *z* directions resulting in a 45° overhang; **b** gyroid scaled by 1.5 in the *z* direction resulting in a 34° overhang; **c** gyroid scaled by 2.0 in the *z* direction resulting in a 27° overhang

of each print. The total print time per overhang test was estimated to be about 35 min.

Figure 6a demonstrates that uniform scaling of the gyroid in all Cartesian directions will have a 45° slope, and when scaled in the vertical direction by 1.5 and 2, the gyroid will have a general slope of 34° and 27°, respectively. However, the general slope does not describe the overhang angle of all the mesh faces within the gyroid geometry. Draft angle analysis can be used to describe each angle of the mesh face relative to the vertical through a color gradient. If 0° is totally vertical and 90° is horizontal, then one can articulate locations of significant overhang between each of the gyroid prototypes through a color gradient (Fig. 7). In Fig. 7, 0°—totally vertical, is all the blue mesh faces and those mesh faces that are most horizontal are colored in red from the perspective of the worm's-eye isometric—an isometric looking up as opposed to down. Each gyroid has a different percentage of mesh faces that are vertical verses horizontal. The angle of each mesh face was rounded to the nearest whole number. Those mesh faces that were totally vertical 0° were culled from the data set to examine only the overhang, 1°–90° and were tallied per each overhang angle (Fig. 8). The graph on Fig. 8 demonstrates that the uniformly scaled prototype had the most significant overhang in which 26% of the mesh faces had more than a 45° overhang. While only 13% of the mesh faces in the gyroid scaled by 1.5 had an overhang beyond 45° and 8% of the mesh faces in the gyroid scaled by 2.0 had an overhang beyond 45°.

4 Results

The research presented demonstrates an NURBS-based modeling method to digitally model gyroid TPMSs. The advantage of this method, as opposed to isosurface-based modeling methods, is that the mesh(s) derived from the NURBS-based modeling method are more uniformly constructed making it a more exact geometry than previously

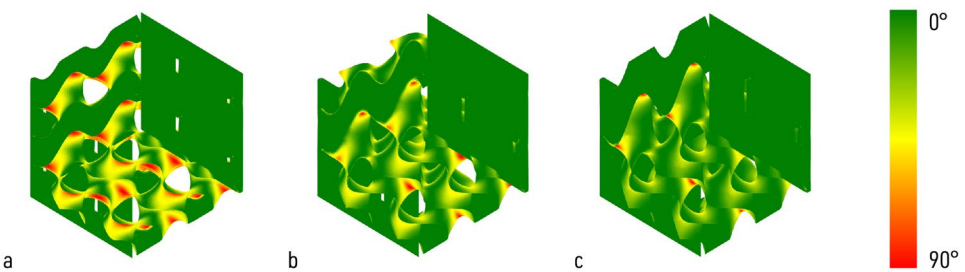

Fig. 7 Worms eye isometric of each gyroid prototype: **a** gyroid uniformly scaled in *x, y*, and *z* directions; **b** gyroid scaled by 1.5 in the *z* direction; **c** gyroid scaled by 2.0 in the *z* direction

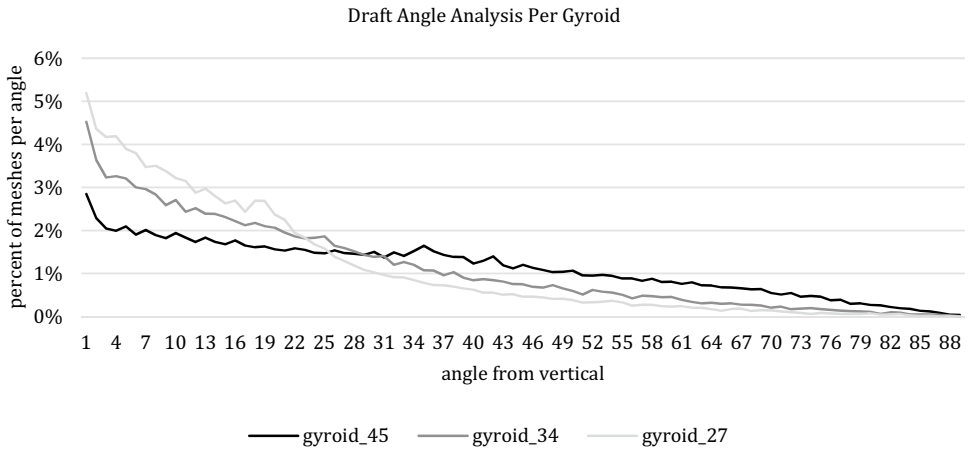

Fig. 8 Draft angle analysis per gyroid prototype: describes the percentage of mesh faces per each overhang angle between 1° and 90° for each prototype

demonstrated by others and can easily be joined with other digital geometry or transformed through various parametric modeling methods. This is not so easy to accomplish with present isosurface modeling methods which can create non-planar naked edges, making it difficult to join with other geometries which also affects the horizontal slicing of the model. Additionally, isosurface modeling methods can create triangulated meshes making it more difficult to orient the first and second directions of orthotropic materials for FEA. In the case of the research presented in this paper, the NURBS-based modeling method was implemented to help construct a continuous toolpath for the gyroid TPMS prototypes.

The 3DPC, used for both the overhang tests and the prototypes for compression testing, maintains its pumping characteristics for at least 20 min without increasing pumping pressures. The in-house developed mixture can be categorized as a high-performance concrete with a compressive strength of 75 MPa at 7 days, 90 MPa at 28 days. With this 3DCP mixture and the extrusion head described in Sect. 3.4, the cantilever tests did demonstrate that a 45° cantilever gyroid TPMS could be printed, however two issues arose during the printing process and immediately following. As mentioned in Sect. 3.3, there were two locations where a 28 mm cantilever was required to keep the tool path continuous, which caused part of the printed prototype to collapse (Fig. 9a). Yet, the equivalent cantilever location on the 34° overhanging prototype only showed mild slumping (Fig. 9b). Additionally, the 45° overhanging gyroid prototype exhibited cracking in the concrete within a few hours after it had been printed (Fig. 9c). It is plausible that the cracking is mostly like the result of the steep overhang within that area. Because the 34° overhanging gyroid showed only mild slumping in the cantilever area and no visible cracking during the curing process, it was selected for compression testing. It should also be noted as it is illustrated in Fig. 6 that the 27° overhang test did not finish printing, because there was a miscalculation in the number of batches required to print all three overhang tests. This miscalculation was a product of the numerous extrusion tests done prior to printing the first overhang test.

Based on the overhanging test, the 34° overhang prototype was selected to investigate the mechanical performance of gyroid cubes under compressive loading. Three identical

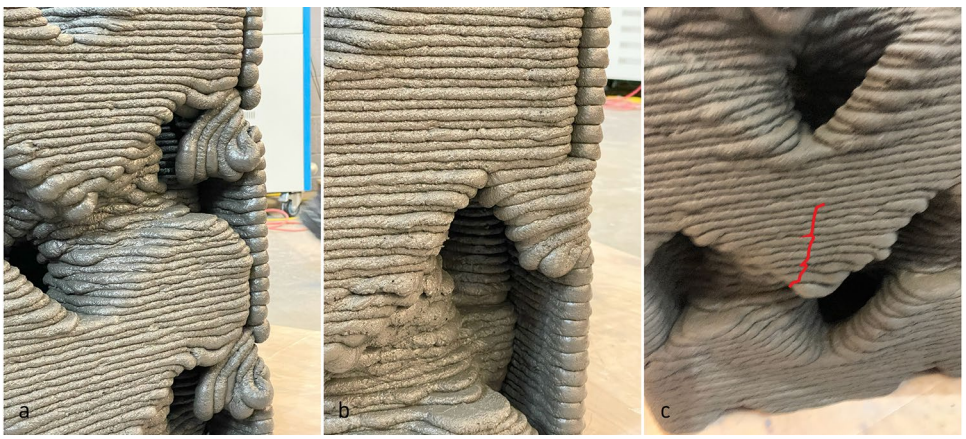

Fig. 9 Photos from 3DPC overhang tests: **a** 28 mm cantilever caused partial collapse of the test; **b** 28 mm cantilever caused minor slumping; **c** 45° overhang test exhibited cracking within hours of fabrication—fracture line is notated in red

34° overhang prototype cubes were printed following the methods described in Sects. 3.4 and 3.5 for compression testing. The printed cubes had an average tool path length of 456 cm per layer and was 28 mm wide, and thus, the average cross section between layers was 1277 cm.^{2}. The theoretical load capacity of the cubes (P_{th}) was estimated considering the cube's cross-sectional area (A_c), and the material's compressive strength (f'_c), as shown in crushing Eq. (3):

$$P_{th} = A_c f'_c. \tag{3}$$

Using Eq. 3, the cubes were found to have a theoretical compressive load capacity of 9475 kN considering the material compressive strength at 7 days of 74.2 MPa. The cubes were moist cured and tested at age of 7 days using a 1780 kN Baldwin Universal Testing Machine with a loading rate of 0.5 mm/min (Fig. 10). The load–displacement curves for the tested gyroid cubes are shown in Fig. 11. The cubes were able to carry a maximum compressive load of 1050 kN, 1275 kN, and 1235 kN with a displacement at maximum load of 5.7 mm, 3.2 mm, and 4.5 mm, respectively. This indicates that the cubes were able to support 11–13% of their theoretical compressive load capacity. However, the theoretical compression capacity does not consider the stress distribution due to gyroid's geometry. As shown in Fig. 10, the cracks run perpendicular to the direction of the direction of the applied load, thereby suggesting that the gyroid prototypes failed due to tensile stress or shear stress.

When comparing the yield stress of the gyroid under compressive and tensile loads, the results are "quasi-identical" (Timercan et al. 2023) or near similar depending on the cellular infill density (Araya et al. 2024). However, in the case of the gyroid prototypes of this paper, 3DPC is the material, which has a high compression strength relative to its tension and shear strengths. According to the Poisson effect, concrete tends to expand laterally when subjected to axial compression loading. The three specimens subjected

Fig. 10 Photos of compression testing

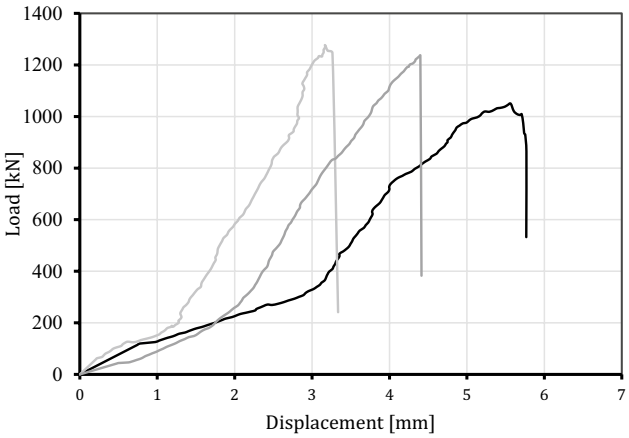

Fig. 11 Results of compression testing

to compression loading in this paper contract between 3.2 and 5.7 mm. Unfortunately, no strain gauges were used to measure the lateral displacement of the specimens, so it is difficult to hypothesize on the exact relationship between axial and transverse strain for each of the gyroid prototypes tested. Furthermore, the interior of the gyroid geometry is quite complex, as illustrated in Fig. 12, making it rather complex to properly apply enough strain gauges to fully and empirically define locations of the high strain. Nonetheless,

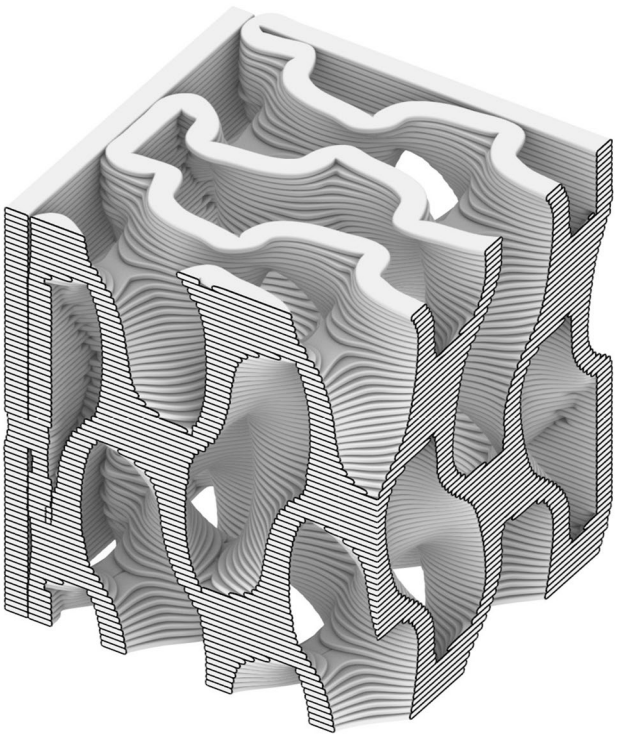

Fig. 12 Section through isometric of 34° gyroid model for 3D printing

it is probable that the varying distribution of local tensile stresses throughout the gyroid prototypes are integral to the mostly vertical cracks in each of the specimens.

Given the loading direction and the percentage of the vertical or near vertical surfaces in the gyroid cubes, it is unlikely that the cubes failed due to pure shear. However, it is possible that local shear failures contributed to the cracking and splitting of the 3DPC in each of the gyroid prototypes. To specify the types of local failures that lead to cracking and splitting in the 3DPC, future FEA is needed to study the stress distribution in 3DPC gyroid structures. The FEA investigation results can also be used for toolpath optimization.

5 Conclusion

The research presented in this paper describes a method to accurately model the gyroid TPMS, such that resulting geometry can easily be joined with NURBS-based geometries or meshes. Due to the fact that the XTreeE mortar extrusion end-effector does not have a start/stop function to pause the flow of the concrete being extruded, a continuous tool path was developed. However, the toolpath design did exhibit several areas in the overhang tests that had a 28 mm cantilever. In the 45° overhang sample, the cantilever existed in two locations, and in the 34° and 27° overhang samples, this condition presented itself twice, once in each sample. Due to the fact that the 27° overhang sample did not finish printing, the cantilevering condition was only exhibited in the digital geometry. Though the compression tests demonstrated that 34° could support up to 1280 times its own self weight, a significant variability was observed between the theoretical and measured values possibly due to internal cracking within each test.

Finite-element analysis will be used in future investigations to structurally simulate and optimize the gyroid geometry for larger 3DPC wall assemblies. Additionally, the toolpath design will be further refined to reduce or eliminate the issue of the 28 mm cantilever exhibited in Fig. 7a, b. Part of this future investigation will also look to develop a continuous toolpath for gyroid-based structures that does not reverse back on itself between layers. The current toolpath travels in opposite directions between odd and even layers. Potentially, layers will have more time to cure if the toolpath is designed to move in the same direction throughout the entirety of the print. Finally, other TPMS surface typologies will be investigated based on different loading scenarios and integration of rebar systems into the printed geometry. Further studies will also examine the probability of cracking during the curing period given various overhang angles to determine a more exact range of allowable overhang angles for doubly curved 3DPC structures.

Acknowledgements The authors would like to thank the School of Civil and Environmental Engineering Department at Cornell University for the use of their robotic printing system and testing facilities located in the Bovay Lab and the College of Architecture, Art, and Planning. This work was supported in part by the Cornell Atkinson Center for Sustainability Academic Venture Fund. We would also like to thank XtreeE for the support received during the development of the printable mixture and the help received from numerous colleagues at Cornell University including Dan Shen, Edie Blaze, Mark Krneta, Nikita Dolgopolov, Pulani Tremel, and John Conrad. Lastly, the authors would like to thank Onur Ozturk for his active review of the work and his future collaborations.

Funding Partial funding was provided by the Cornell Atkinson Center for Sustainability Academic Venture Fund.

Data availability The data associated with the current study are available from the corresponding author upon reasonable request.

Declarations

Conflict of interest On behalf of all authors, the corresponding author states that there is no conflict of interest.

References

Akbarzadeh M et al (2024) Diamanti: 3D-printed, post-tensioned concrete canopy. In: Fabricate 2024, in creating resourceful futures. UCL Press, 2024, pp 292–301. https://doi.org/10.2307/j.ctv13xpsvw.19

Al-Ketan O, Abu Al-Rub RK (2021) MSLattice: a free software for generating uniform and graded lattices based on triply periodic minimal surfaces. Mater Des Process Commun 3(6):e205. https://doi.org/10.1002/mdp2.205

Anton A, Reiter L, Wangler T, Frangez V, Flatt RJ, Dillenburger B (2021) A 3D concrete printing prefabrication platform for bespoke columns. Autom Constr 122:103467. https://doi.org/10.1016/j.autcon.2020.103467

Araya M, Jaskari M, Rautio T, Guillén T, Järvenpää A (2024) Assessing the compressive and tensile properties of TPMS-Gyroid and stochastic Ti64 lattice structures: a study on laser powder bed fusion manufacturing for biomedical implants. J Sci Adv Mater Dev 9(1):100663. https://doi.org/10.1016/j.jsamd.2023.100663

Carneau P, Mesnil R, Roussel N, Baverel O (2019) An exploration of 3d printing design space inspired by masonry.10.5281/zenodo.3563672

Conrad J et al (2023) Concrete printed gyroid column: a structurally optimized, sand layer supported printing method. In: Proceedings of the 41st eCAADe conference, Graz, Austria (forthcoming)

Darweesh B, Rael R (2024) From walls to roofs: formwork-free robotic earthen vault construction. In: Fabricate 2024, in creating resourceful futures. UCL Press, pp 172–179. https://doi.org/10.2307/j.ctv13xpsvw.19

Dell'Endice A, Bouten S, Van Mele T, Block P (2023) Structural design and engineering of Striatus, an unreinforced 3D-concrete-printed masonry arch bridge. Eng Struct 292:116534. https://doi.org/10.1016/j.engstruct.2023.116534

Downing D, Jones A, Brandt M, Leary M (2021) Increased efficiency gyroid structures by tailored material distribution. Mater Des 197:109096. https://doi.org/10.1016/j.matdes.2020.109096

du Plessis A, Babafemi AJ, Paul SC, Panda B, Tran JP, Broeckhoven C (2021) Biomimicry for 3D concrete printing: a review and

perspective. Addit Manuf 38:101823. https://doi.org/10.1016/j.addma.2020.101823
Duarte G, Brown N, Memari A, Duarte JP (2021) Learning from historical structures under compression for concrete 3D printing construction. J Build Eng 43:103009. https://doi.org/10.1016/j.jobe.2021.103009
Flores-Jimenez MS, Delgado-Gutiérrez A, Fuentes-Aguilar RQ, Cardenas D (2022) Generation of a quadrilateral mesh based on NURBS for gyroids of variable thickness and porosity. J Appl Comput Mech 8(2):684–698. https://doi.org/10.22055/jacm.2021.38645.3260
Gandy PJF, Klinowski J (2000) Exact computation of the triply periodic G ('Gyroid') minimal surface. Chem Phys Lett 321(5):363–371. https://doi.org/10.1016/S0009-2614(00)00373-0
Gibson LJ (2003) Cellular solids. MRS Bull 28(4):270–274. https://doi.org/10.1557/mrs2003.79
Gibson LJ, Ashby MF, Harley BA (2010) Cellular materials in nature and medicine. In: Cellular materials in nature and medicine. University Press, Cambridge
Jipa A, Dillenburger B (2022) 3D printed formwork for concrete: state-of-the-art, opportunities, challenges, and applications. 3D Print Addit Manuf 9(2):84–107. https://doi.org/10.1089/3dp.2021.0024
Joedicke J (1963) Shell architecture. Reinhold Publishing Corporation, New York
Ko C-H, Kuo J-D (2019) Making formwork design lean. J Eng Proj Prod Manag 9(1):29–47. https://doi.org/10.2478/jeppm-2019-0005
Li Z, Chen Z, Chen X, Zhao R (2022) Effect of surface curvature on the mechanical and mass-transport properties of additively manufactured tissue scaffolds with minimal surfaces. ACS Biomater Sci Eng 8(4):1623–1643. https://doi.org/10.1021/acsbiomaterials.1c01438
Liu J, Nguyen-Van V, Panda B, Fox K, Plessis A, Tran P (2022) Additive manufacturing of sustainable construction materials and form-finding structures: a review on recent progresses. 3D Print Addit Manuf 9(1):12–34. https://doi.org/10.1089/3dp.2020.0331
Lok L, Zivkovic S, Meyer-Brötz F, Zerbe H (2024) House of cores. In: Fabricate 2024, in creating resourceful futures. UCL Press, pp 172–179. https://doi.org/10.2307/j.ctv13xpsvw.19
Maskery I, Aremu AO, Parry L, Wildman RD, Tuck CJ, Ashcroft IA (2018) Effective design and simulation of surface-based lattice structures featuring volume fraction and cell type grading. Mater Des 155:220–232. https://doi.org/10.1016/j.matdes.2018.05.058
Nguyen-Van V, Tran P, Peng C, Pham L, Zhang G, Nguyen-Xuan H (2020) Bioinspired cellular cementitious structures for prefabricated construction: hybrid design & performance evaluations. Autom Constr 119:103324. https://doi.org/10.1016/j.autcon.2020.103324
Paul SC, van Zijl GPAG, Tan MJ, Gibson I (2018) A review of 3D concrete printing systems and materials properties: current status and future research prospects. Rapid Prototyp J 24(4):784–798. https://doi.org/10.1108/RPJ-09-2016-0154
Robert McNeel & Associates (2022) Rhino3d. Robert McNeel & Associates
Rutten D (2022) Grasshopper. Robert McNeel & Associates. [Windows]. https://www.grasshopper3d.com/
Sadoc JF, Charvolin J (1989) Infinite periodic minimal surfaces and their crystallography in the hyperbolic plane. Acta Crystallogr A Found Crystallogr 45(1):10–20. https://doi.org/10.1107/S0108767388008438
Schoen AH (1970) Infinite periodic minimal surfaces without self-intersections. National Aeronautics and Space Administration, Washington, D.C., NASA Technical Note NASA TN D-5541
Timercan A, Terriault P, Brailovski V (2023) Axial tension/compression and torsional loading of diamond and gyroid lattice structures for biomedical implants: simulation and experiment. Mater Des 225:111585. https://doi.org/10.1016/j.matdes.2022.111585
Vantyghem G, De Corte W, Shakour E, Amir O (2020) 3D printing of a post-tensioned concrete girder designed by topology optimization. Autom Constr 112:103084. https://doi.org/10.1016/j.autcon.2020.103084
Viswanath A, Khan KA, Barsoum I (2022) Design of novel isosurface strut-based lattice structures: effective stiffness, strength, anisotropy and fatigue properties. Mater Des 224:111293. https://doi.org/10.1016/j.matdes.2022.111293
Wakefield E (2023) 3D printed Smart Bridge unveiled at Autodesk University 2022, VoxelMatters—the heart of additive manufacturing. [Online]. https://www.voxelmatters.com/3d-printed-smart-bridge-unveiled-at-autodesk-university-2022/. Accessed 31 Mar 2023
Xiao J et al (2021) Large-scale 3D printing concrete technology: current status and future opportunities. Cem Concr Compos 122:104115. https://doi.org/10.1016/j.cemconcomp.2021.104115
Yabanigül MN, Yazar T (2021) Production of Gyroid-like modular systems with non-linear robotic hotwire cutting. Autom Constr 126:103671. https://doi.org/10.1016/j.autcon.2021.103671
Zhang B, Mhapsekar K, Anand S (2017) Design of variable-density structures for additive manufacturing using gyroid lattices. In: IDETC-CIE2017, volume 4: 22nd design for manufacturing and the life cycle conference; 11th international conference on micro- and nanosystems. https://doi.org/10.1115/DETC2017-68047